



HAL
open science

Synthesis, Structure, and Electrochemical Properties of Sterically Protected Molybdenum Trihydride Redox Pairs: A Paramagnetic “Stretched” Dihydrogen Complex?

Miguel Baya, Jennifer Houghton, Jean-Claude Daran, Rinaldo Poli, Louise Male, Alberto Albinati, Matthias Gutman

► To cite this version:

Miguel Baya, Jennifer Houghton, Jean-Claude Daran, Rinaldo Poli, Louise Male, et al.. Synthesis, Structure, and Electrochemical Properties of Sterically Protected Molybdenum Trihydride Redox Pairs: A Paramagnetic “Stretched” Dihydrogen Complex?. *Chemistry - A European Journal*, 2007, 13 (19), pp.5347-5359. 10.1002/chem.200700293 . hal-03194007

HAL Id: hal-03194007

<https://hal.science/hal-03194007>

Submitted on 9 Apr 2021

HAL is a multi-disciplinary open access archive for the deposit and dissemination of scientific research documents, whether they are published or not. The documents may come from teaching and research institutions in France or abroad, or from public or private research centers.

L'archive ouverte pluridisciplinaire **HAL**, est destinée au dépôt et à la diffusion de documents scientifiques de niveau recherche, publiés ou non, émanant des établissements d'enseignement et de recherche français ou étrangers, des laboratoires publics ou privés.

**Synthesis, structure and electrochemical properties of sterically protected
molybdenum trihydride redox pairs: A paramagnetic “stretched”
dihydrogen complex?**

Miguel Baya,^a Jennifer Houghton,^a Jean-Claude Daran,^a Rinaldo Poli,^{*a} Louise Male,^b

Alberto Albinati^b and Matthias Guttman,^c

^a*Laboratoire de Chimie de Coordination, UPR CNRS 8241 liée par convention à l'Université Paul Sabatier et à l'Institut National Polytechnique de Toulouse, 205 Route de Narbonne, 31077 Toulouse Cedex, France*

^b*Department of Structural Chemistry (DCSSI), Università di Milano, Via G. Venezian 21, 20133 Milano, Italy.*

^c*Rutherford Appleton Laboratory, ISIS Facility, Chilton (Didcot) OX11 0QX U.K..*

Proofs to:

Rinaldo Poli

Tel: +33-561333173

Fax: +33-561553003

E-mail: poli@lcc-toulouse.fr

Summary

Complexes $\text{Cp}^{\#}\text{Mo}(\text{PMe}_3)_2\text{H}_3$ ($\text{Cp}^{\#} = 1,2,4\text{-C}_5\text{H}_2t\text{Bu}_3$, **2a**; $\text{C}_5\text{H}_i\text{Pr}_4$, **2b**) have been synthesized from the corresponding compounds $\text{Cp}^{\#}\text{MoCl}_4$ (**1a**, **1b**) and fully characterized, including by X-ray crystallography and by a neutron diffraction study for **2a**. Protonation of **2a** led to complex $[(1,2,4\text{-C}_5\text{H}_2t\text{Bu}_3)\text{Mo}(\text{PMe}_3)_2\text{H}_4]^+$ (**3a**) in THF and to $[(1,2,4\text{-C}_5\text{H}_2^i\text{Bu}_3)\text{Mo}(\text{PMe}_3)_2(\text{MeCN})\text{H}_2]^+$ (**4a**) in MeCN. Complex **4b** analogously derives from protonation of **2b** in MeCN, whereas the tetrahydride complex **3b** is unstable. One-electron oxidation of **2a** and **2b** by $[\text{Cp}_2\text{Fe}]\text{PF}_6$ produces the EPR active 17-electron complexes $[\mathbf{2a}]^+$ and $[\mathbf{2b}]^+$. The former is thermally more stable than the latter and could be crystallographically characterized as the PF_6^- salt by X-ray diffraction, providing evidence for the presence of a stretched dihydrogen ligand ($\text{H}\cdots\text{H} = 1.36(6) \text{ \AA}$). Controlled thermal decomposition of $[\mathbf{2a}]^+$ yielded the product of H_2 elimination, the 15-electron monohydride complex $[(1,2,4\text{-C}_5\text{H}_2t\text{Bu}_3)\text{Mo}(\text{PMe}_3)_2\text{H}]\text{PF}_6$ (**5a**) which was characterized by X-ray crystallography and by EPR spectroscopy at liquid He temperature. The compound establishes an equilibrium with the solvent adduct in THF. An electrochemical study by cyclic voltammetry provides further evidence for a rapid H_2 elimination process from the 17-electron complexes. Contrary to the previously investigated $[\text{Cp}^*\text{Mo}(\text{dppe})\text{H}_3]^+$ system, the decomposition of $[\mathbf{2a}]^+$ by H_2 substitution with a solvent molecule appears to follow a dissociative pathway in MeCN.

Keywords

Molybdenum, bulky cyclopentadienyl ligands, hydride ligands, paramagnetic hydride complexes, oxidatively induced reductive elimination, neutron diffraction

Introduction

Hydride complexes have paramount importance in light of their implication in a variety of catalytic processes and as models of a number of biological functions such as hydrogenase and nitrogenase.^[1-6] Because of the strong covalent nature of the M-H σ bond and the absence of additional orbital interactions (*i.e.* of π type), they are usually stable only in a closed-shell configuration. Open-shell versions are reactive, which is the very reason for their involvement as catalytic intermediates. An interesting subclass of open-shell hydride complexes are those with an odd-electron (mostly 17-electron) configuration, characterized by paramagnetism. These complexes have generally been accessed by one-electron oxidation of stable diamagnetic precursors. In most cases, they decompose by deprotonation,^[7] disproportionation,^[8] dihydrogen reductive elimination (for complexes containing at least two hydride ligands),^[9] atom transfer,^[10] and other pathways.^[11] This multitude of available reaction pathways complicates their potential application, for instance in electrocatalysis. It is therefore useful to investigate in greater detail how the various pathways depend on the reaction conditions (*e.g.* solvent, available substrates) and molecular parameters (*e.g.* stereoelectronic properties of the ligand environment). For this purpose, it is necessary to develop more stable systems. We have learned from previous investigations^[9, 12-16] that all decomposition pathways are disfavored by both a stronger electron donating and more sterically protecting ligand environment.

The oxidation of Cp*Mo(dppe)H₃ (dppe = Ph₂PCH₂CH₂PPh₂) was studied in the greatest detail.^[9, 12, 16] It leads to the paramagnetic complex [Cp*Mo(dppe)H₃]⁺, which is stable at low temperatures and was characterized *in situ* by EPR spectroscopy. The detailed investigation of its decomposition at room temperature enabled us to quantify the relative rates of deprotonation (by the residual neutral precursor), disproportionation, and H₂

elimination in various solvents.^[9, 16] This was the first reported example where H₂ oxidatively induced reductive elimination could be unambiguously demonstrated and distinguished from other decomposition pathways. Oxidation of a polyhydride complex {MH_n} is expected to favor its rearrangement to a nonclassical isomer, {MH_{n-2}(H₂)}⁺,^[17, 18] but the multitude of decomposition pathways, all possibly leading to H₂ evolution,^[19] have previously made the identification of the H₂ elimination pathway uncertain.^[17, 20] For this specific trihydrido molybdenum complex all three decomposition pathways were shown to occur via the nonclassical intermediate [Cp*Mo(dppe)H(H₂)]⁺, although theoretical calculations and circumstantial evidence indicates that the oxidized complex adopts a classical structure. Since the nonclassical tautomer is energetically less accessible for the related tungsten system, complex [Cp*W(dppe)H₃]⁺ turned out to be sufficiently stable to be isolated and crystallographically characterized.^[9]

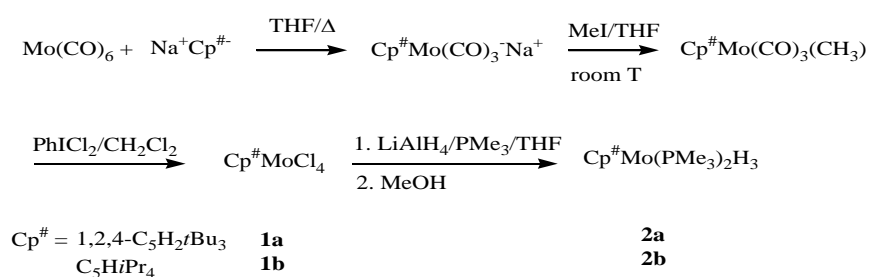
In this contribution, we report the synthesis and investigations into new molybdenum systems, isoelectronic with Cp*Mo(dppe)H₃, that contain an even more strongly donating and sterically encumbering coordination sphere. We used the two highly substituted cyclopentadienyl rings, C₅H₄iPr₄ and 1,2,4-C₅H₂*t*Bu₃, in place of Cp* and two PMe₃ ligands in place of bidentate dppe. Notable results of this investigation have been the isolation and structural characterization of the 17-electron oxidation product, [(1,2,4-C₅H₂*t*Bu₃)Mo(PMe₃)₂H₃]⁺, and the observation of its subsequent H₂ elimination process leading to the 15-electron monohydride derivative, [(1,2,4-C₅H₂*t*Bu₃)Mo(PMe₃)₂H]⁺, which was also structurally characterized. Some aspects of this investigation have been recently communicated.^[21] While those preliminary results will be reported again here in fuller details, stronger emphasis will be placed on complementary investigations that have not previously been described.

Results and Discussion

(a) Synthesis and characterization of the diamagnetic trihydride complexes

$\text{Cp}^\# \text{Mo}(\text{PMe}_3)_2\text{H}_3$ ($\text{Cp}^\# = 1,2,4\text{-C}_5\text{H}_2\text{tBu}_3$, **2a**; $\text{C}_5\text{H}_i\text{Pr}_4$, **2b**)

Adaptation of Schrock's Cp^*MoCl_4 synthetic procedure^[22, 23] to the bulkier $\text{Cp}^\#$ analogues ($\text{Cp}^\# = 1,2,4\text{-C}_5\text{H}_2\text{tBu}_3$, **a**, and $\text{C}_5\text{H}_i\text{Pr}_4$, **b**) yielded the corresponding $\text{Cp}^\#\text{MoCl}_4$ derivatives **1a** and **1b** in good yields, see Scheme 1. Subsequent reaction of these compounds with LiAlH_4 in the presence of ≥ 2 equivalents of PMe_3 , followed by methanolysis and crystallization from ether, yielded the corresponding trihydride derivatives, $\text{Cp}^\#\text{Mo}(\text{PMe}_3)_2\text{H}_3$, **2a** and **2b**. It is interesting to compare these results with that previously reported for the related Cp^* system, which led to a mixture of $\text{Cp}^*\text{Mo}(\text{PMe}_3)_2\text{H}_3$ and $\text{Cp}^*\text{Mo}(\text{PMe}_3)_3\text{H}$.^[24] The bulkier $\text{Cp}^\#$ systems afford the trihydride derivatives **2** selectively and show no tendency to replace H_2 in the presence of excess PMe_3 under thermolytic conditions.



Scheme 1

Both compounds gave single crystals suitable for a structural analysis. The crystal of **2a** had sufficient quality to allow the location and refinement of the hydride positions from the X-ray data, as shown in the previous communication.^[21] We have now completed the structural investigation with a neutron diffraction experiment for **2a** (the results of both refinements are compared in Table 1) and an X-ray diffraction experiment for **2b**. The latter

crystals had poorer quality and the hydride positions could not be located; the observable structural parameters are very close to those of **2a**, see Table 1. A view of both geometries is shown in Figure 1. The molecular geometry is unusual for a half sandwich (ring)MoX₃L₂ compound, but parallels that previously reported for the related Cp*MoH₃(dppe) compound.^[25, 26] This demonstrates that the unusual structure observed for Cp*MoH₃(dppe) is not enforced by the chelating nature of the dppe ligand. Another example for this structural type has recently been reported for the isoelectronic compound Cp*W(CO)₂H₂(SiH₂Ph).^[27] As expected, the X-ray diffraction experiment yields shorter Mo-H distances than the neutron diffraction experiment for compound **2a**. Only those afforded by neutron diffraction should be considered reliable. The parameters that do not involve hydrogen atom positions, on the other hand, are more precisely determined by the X-ray diffraction experiment.

The most interesting structural feature is the distance between atoms H2 and H3 [1.69(2) Å from the neutron structure]. This value is too long to envisage an interaction, but short in comparison to most nonbonded distances recorded by neutron diffraction for polyhydride complexes. This is evidence for a certain degree of “compression”.^[28] Other relatively short nonbonded H···H separations are 1.67(1) and 1.70(1) Å in [CpIr(PMe₃)H₃]⁺,^[29] and values ranging from 1.637(4) to 1.668(4) Å between adjacent H atoms in compound Os(PiPr₂Ph)₂H₆,^[30] whereas there are no shorter intramolecular H···H separations than 1.77 Å in compound Re(dppe)H₇.^[31] The longest H-H separations in compounds that have been defined as “stretched H₂ complexes” are 1.357(7) Å in ReH₇(P(C₆H₄-*p*-CH₃)₃)₂^[32] and 1.34(2) in [Os(H₂)(en)₂(O₂CMe)]⁺PF₆⁻,^[33] all these values resulting again from neutron diffraction experiments. Finally, complex OsH₅(PMe₂Ph)₃⁺ exhibits an even longer separation (1.49(4) Å) and was described as falling in a “gray” region where there may or may not be a direct H/H attractive interaction.^[34] The Cambridge Crystallographic Structural Database does not reveal H-H contacts between 1.0 and 1.7 Å for

Mo complexes, but a distance of ca. 1.18 Å has recently been estimated from T_1 and J_{HD} measurements for complex $[\text{Mo}(\text{NPh})(\text{PMe}_3)_2(\text{H}_2)(o\text{-(Me}_3\text{SiN)}_2\text{C}_6\text{H}_4)]$.^[35] Interestingly, if the H2 and H3 atoms are considered as defining a stretched H_2 ligand, therefore occupying a single coordination position in a Mo^{II} complex, then the coordination geometry would be described as a “four-legged piano stool”, which is indeed a quite common geometrical arrangement for Mo^{II} ,^[36] as exemplified by $\text{CpMo}(\text{PMe}_2\text{Ph})_3\text{Cl}$ ^[37] and $\text{CpMo}(\text{dppe})(\text{CO})\text{H}$.^[38]

<Table 1>

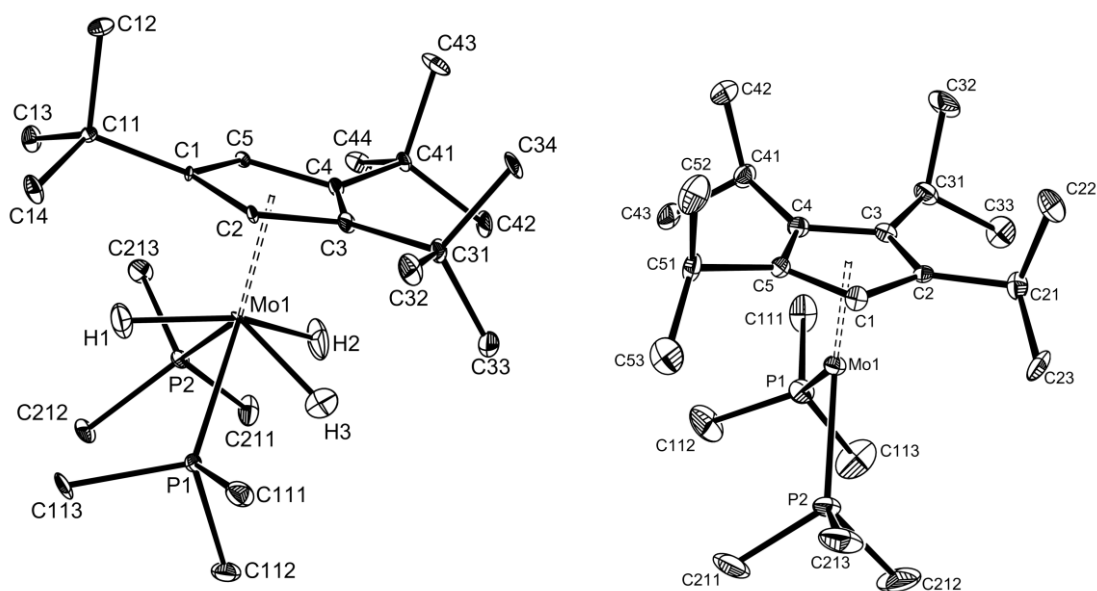


Figure 1. ORTEP view of compounds **2a** (neutron diffraction, left) and **2b** (right). Hydrogen atoms, except those directly bonded to the Mo atom in compound **2a**, are not shown for clarity.

The NMR properties of **2a** and **2b** confirm the presence of three hydride ligands. The single $^{31}\text{P}\{^1\text{H}\}$ resonance observed at room temperature is transformed into a binomial quartet in a $^{31}\text{P}\{\text{sel. } ^1\text{H}\}$ NMR experiment, showing that the P nuclei are coupled to three equivalent protons. In addition, the ^1H spectrum shows a single, sharp triplet resonance. A rapid

exchange process between the inequivalent hydride positions must therefore be present. For the related Cp*Mo(dppe)H₃ compound, the fluxional process could not be frozen out even at the lowest attainable temperatures.^[26] For compounds **2a** and **2b**, on the other hand, cooling results in decoalescence for the ¹H NMR signal to yield two signals in a 1:2 ratio, consistent with the solid state structural investigation, see Figure 2. This shows quite clearly the effect of the bulky ring substituents on the dynamics of the hydride exchange process. For compound **2a**, the lowest temperature (193 K) spectrum displayed well resolved triplets, due to coupling to the two equivalent P donor nuclei, with the unique hydride ligand being characterized by a greater J_{HP} (64 Hz), relative to the two equivalent ones (44 Hz). No H-H coupling between the inequivalent hydrides can be discerned. For compound **2b**, on the other hand, the spectrum remained rather broad even at 193 K. A lineshape analysis yielded the activation parameters of the hydride scrambling process as $\Delta H^\ddagger = 9.0 \pm 0.7$ (**2a**) and 8.5 ± 0.3 (**2b**) kcal mol⁻¹; $\Delta S^\ddagger = 17 \pm 3$ (**2a**) and 21 ± 1 (**2b**) e.u. The similar values of both activation parameters for the two compounds are in line with the similar structure of the two compounds. The longitudinal relaxation times (T₁) of the various signals are also shown in Figure 2. They confirm the classical nature of the compounds. Most notably, for compound **2a**, the T₁ value for the equivalent hydride ligands signal is not significantly shorter than that of the unique hydride resonance below the decoalescence temperature.

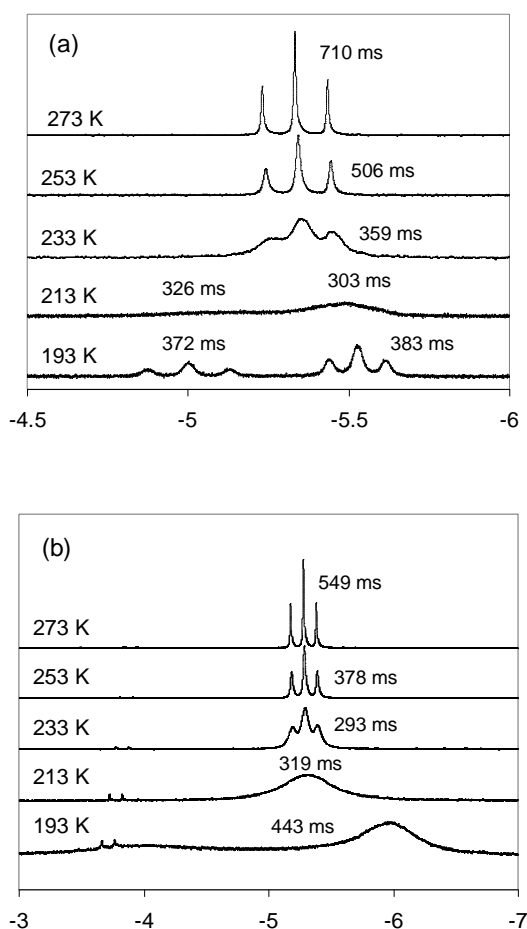


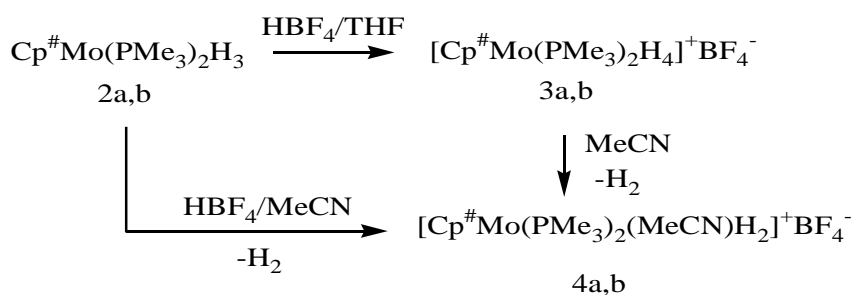
Figure 2. Variable temperature ¹H NMR spectrum of (a) compound **2a** and (b) compound **2b** in the hydride resonance region. The individual temperatures are shown on each spectrum and the time values shown are the longitudinal relaxation times of the corresponding resonance.

The ³¹P NMR resonance of the two phosphine ligands remained sharp in the entire temperature range for compound **2a**, in agreement with the chemical equivalence shown by the X-ray structure. For compound **2b**, on the other hand, a decoalescence phenomenon was observed at low temperatures, yielding two singlet resonances with approximately equal intensities at δ 15.9 and 12.3 at 193 K (Figure shown in the Supporting Information). This behaviour can be rationalized by either the freezing out of a single Mo-(C₅H₇Pr₄) rotamer with symmetry inequivalent PMe₃ donors (but these ligands also need to be characterized by a small enough P-P coupling since this is not observed at 193 K), or by the presence of two

equilibrating rotamers having similar energy, perhaps differing by the relative conformation of the *i*Pr groups in the C₅H*i*Pr₄ ring. The latter phenomenon would not be expected to lead to the existence of different rotamers for the 1,2,4-C₅H₂*t*Bu₃ substituted complex.

(b) Protonation studies

Compound **2a** reacts with HBF₄ at -80°C in THF to yield the tetrahydride complex [(1,2,4-C₅H₂*t*Bu₃)MoH₄(PMe₃)₂]⁺BF₄⁻, **3a**, see Scheme 2. This product is related to the previously described [Cp*Mo(dppe)H₄]⁺,^[26] but shows a much greater thermal stability. It is stable in THF solution at room temperature, whereas complex [Cp*Mo(dppe)H₄]⁺ decomposes rapidly by loss of H₂ via a presumed nonclassical [Cp*Mo(dppe)(H₂)H₂]⁺ intermediate. This stabilization effect is probably related to the greater donor power of the coordination sphere in **3a** relative to [Cp*Mo(dppe)H₄]⁺, with the corresponding stabilization of the classical tetrahydrido structure with respect to the nonclassical tautomer. Compound **3a** is diamagnetic and colorless, as expected for the *d*⁰ configuration of formally hexavalent molybdenum. It features, as expected, a triplet hydride signal in the ¹H NMR spectrum (at -4.2 ppm) and a singlet (at 0.6 ppm) in the ³¹P{¹H} NMR spectrum. Selective irradiation of the PMe₃ proton resonance yields a quintet ³¹P signal, in agreement with the presence of four hydride ligands. The compound has also been structurally characterized by single crystal X-ray diffraction.



Scheme 2

The cation geometry is illustrated in Figure 3. The crystal quality allowed the location and refinement of all four hydride ligands. The geometry of the tetrahydride cation can be described as a highly distorted pentagonal bipyramid, when the bulky (1,2,4- $C_5H_2tBu_3$) ligand is considered to occupy a single coordination position at one of the vertices of the bipyramid. The second axial position is occupied by the hydride ligand H4, with the 5 equatorial ligands bent toward H4 and away from the cyclopentadienyl ligand (especially the two phosphine ligands, for steric reasons). The two PMe_3 ligands occupy 1,3 positions in the pseudo-pentagonal plane, with atom H1 bisecting the P1-Mo-P2 angle. The related complex $[Cp^*W(dppe)H_4]^+$ was found to adopt an analogous coordination geometry, with the chelating dppe ligand occupying one equatorial and one axial site.^[26]

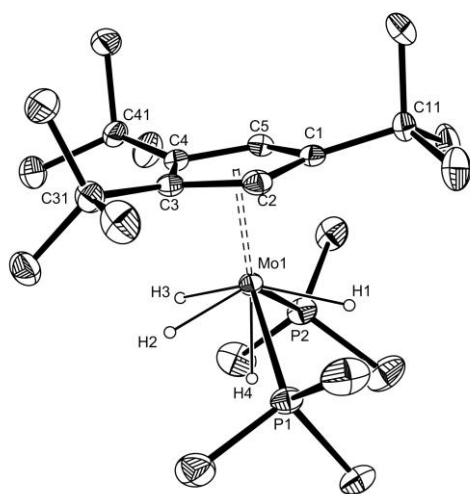
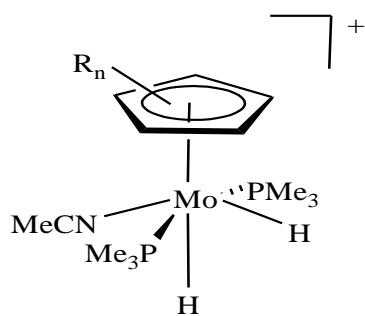


Figure 3. ORTEP view of the cation in compound **3a**. Hydrogen atoms, except those directly bonded to the Mo atom, are not shown for clarity.

The cationic tetrahydride complex **3a** was also formed by protonation of **2a** with HBF_4 in MeCN, but further rapid evolution took place in this case. This reaction was only carried out on a spectroscopic scale in CD_3CN and the resulting solution was monitored with time by

^1H and ^{31}P NMR spectroscopy. Within minutes at room temperature, resonances corresponding to a second complex began to appear and the conversion was complete in 5 h. This product, $[(1,2,4\text{-C}_5\text{H}_2^t\text{Bu}_3)\text{Mo}(\text{PMe}_3)_2(\text{MeCN})\text{H}_2]^+$, **4a**, derives from H_2 elimination/MeCN coordination from **3a**. It displays a singlet $^{31}\text{P}\{^1\text{H}\}$ resonance at 1.85 ppm, which converts into a triplet upon selective decoupling of the PMe_3 ligand ^1H resonance. At room temperature a single broad hydride resonance is observed, however on cooling a CD_3CN solution to -40°C , two triplet hydride resonances are resolved at -0.27 and -6.77 ppm respectively. This suggests that the two PMe_3 ligands occupy equivalent positions at all temperatures, consistent with the structure shown in **I**.



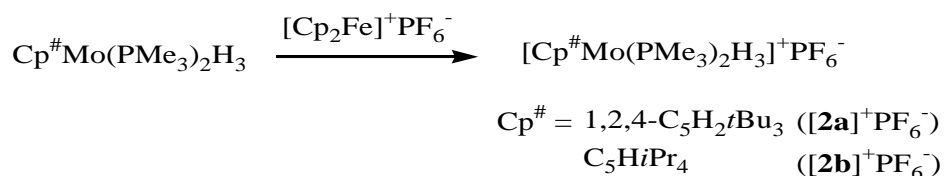
I $\text{R}_n = 1,2,4\text{-}t\text{Bu}_3, i\text{Pr}_4$

The corresponding reaction of **2b**, when carried out in THF at -80°C , led to the precipitation of a white solid, presumably corresponding to the $[(\text{C}_5\text{HiPr}_4)\text{Mo}(\text{PMe}_3)_2\text{H}_4]^+$ complex, **3b**. However, this compound decomposes, even in the solid state, when warmed up to room temperature. Therefore, it could not be spectroscopically characterized. When the same protonation reaction was carried out in acetonitrile, the formation of complex $[(\text{C}_5\text{HiPr}_4)\text{Mo}(\text{PMe}_3)_2(\text{MeCN})\text{H}_2]^+$, **4b**, could be observed. As with **4a**, the hydride ligands in complex **4b** are involved in a fluxional process at room temperature, appearing as a very broad resonance at -2.5 ppm. On cooling to 200 K in acetone- d_6 , two doublet of triplet resonances decoalesce, at -0.13 and -5.27 ppm respectively, confirming that each hydride

ligand couples to two equivalent phosphorus nuclei and to the other hydride ligand, in agreement with structure **I**. At this temperature, all four isopropyl groups on the cyclopentadienyl moiety also become inequivalent. In both complexes **4**, a resonance integrating to 3 protons, assigned to the coordinated MeCN, can be observed at δ 2.17 (for **4a** in CD₃CN) and 2.71 (for **4b** in acetone-*d*₆). This behaviour is analogous to that of the related Cp*Mo(dppe)H₃ complex.^[26] The greater coordinating ability of the acetonitrile solvent induces a more facile H₂ elimination by more efficiently trapping the resulting 16-electron fragment.

(c) Oxidation studies: isolation and characterization

Preliminary electrochemical investigations indicated that both complexes **2a,b** undergo an electrochemically reversible one-electron oxidation process and suggested that the oxidation product is relatively stable. The electrochemical behavior will be analysed in more detail later in section (e). The stoichiometric oxidation was accomplished by the use of Cp₂Fe⁺PF₆⁻ in THF, see Scheme 3. The product for the 1,2,4-C₅H₂*t*Bu₃ system was sufficiently stable to be isolated and crystallized. Its X-ray structure and its EPR spectrum (Figure 4) demonstrate its chemical identity as the PF₆⁻ salt of the one-electron oxidation product, [**2a**]⁺, as discussed previously.^[21]



Scheme 3

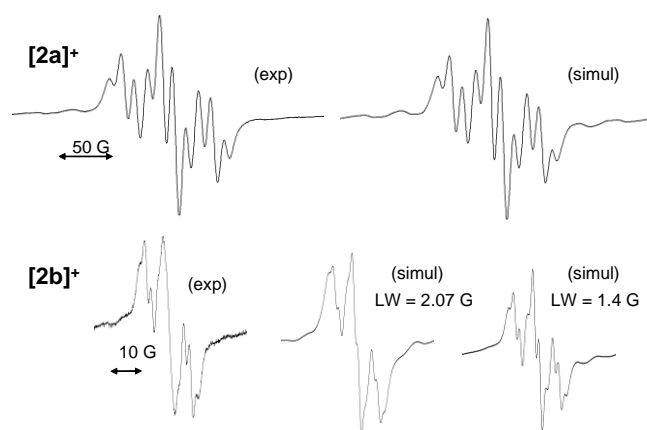


Figure 4. EPR spectra of complexes $[2]^+$ in THF solution. Above: complex $[2a]^+$ ($T = 193$). Below: complex $[2b]^+$ ($T = 183$).

The most relevant metric parameters of the $[2a]^+$ structure are compared with those of the parent compound **2a** in Table 1. The overall geometry of the cation is essentially unchanged relative to that of the neutral precursor (see the previous communication for an ORTEP view).^[21] There is no evidence of an interaction between the two ions, notably hydrogen bonding between the hydride ligands and the fluorine atoms of the anion. The Mo-CNT distance is slightly shorter, whereas the Mo-P distances is slightly longer, relative to the neutral precursor. The most notable change is a decrease of the H2 \cdots H3 contact from 1.69(2) Å (neutron diffraction) or 1.63(4) Å (X-ray diffraction) in the neutral complex to an average of 1.36(6) Å (from the X-ray data) in the cation. The difference is significant at the 2σ level relative to the X-ray structure, at the 4σ level relative to the neutron structure. Unfortunately, suitable crystals of compound $[2a]^+PF_6^-$ for a neutron diffraction analysis could not be grown. Even when keeping the uncertainty into account, however, the H2 \cdots H3 separation in the cationic complex falls inside the range of compounds that have previously been described as “stretched” or “elongated” dihydrogen complexes, or alternatively as “compressed” dihydrides.^[28, 39] Thus, it appears that the oxidation process has increased the interaction between the two hydride ligands H2 and H3.

Compound $[\mathbf{2a}]^+\text{PF}_6^-$ appears to be the first reported paramagnetic polyhydride complex showing evidence for a stretched dihydrogen ligand (or compressed MH_2 system). It is interesting to compare this structure with that of the previously published isoelectronic $[\text{Cp}^*\text{W}(\text{dppe})\text{H}_3]^+$ complex. The two systems show a very different arrangement of the three hydride ligands, the closest $\text{H}\cdots\text{H}$ contact in the tungsten complex being 2.11 Å.^[9] Although the H positions in this tungsten complex should again be considered with caution since this structure was also obtained from X-ray diffraction data, the relative arrangement of the heavy atoms that define the coordination sphere (the Cp ring, the metal, and the P donor atoms) is quite different in the two compounds. As we know, the W complex is stable and has no tendency to decompose, notably by H_2 elimination.

The oxidation product obtained from $\mathbf{2b}$ is rather short-lived at room temperature and could not be isolated. It was only characterized *in situ* by EPR spectroscopy, see Figure 4. Like $[\mathbf{2a}]^+$, it exhibits a rather broad spectrum at ambient temperature, which become sufficiently resolved at lower temperatures to allow the identification of the expected quartet of triplet feature, consistent with the presence of two phosphorus donor atoms and three hydride ligands, flanked by the ^{95}Mo and ^{98}Mo isotope satellites. This suggests, like for the 1,2,4-*t*Bu₃ analogue, that one-electron oxidation has afforded complex $[\mathbf{2b}]^+$.

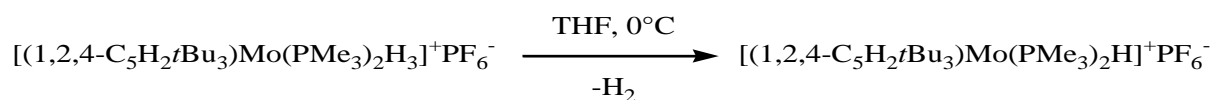
The spectroscopic properties, however are peculiar in many respects. The simulation on the basis of any combination of spin $\frac{1}{2}$ nuclei different than P_2H_3 (for instance, 2 P and 2 H) failed to provide a spectrum sufficiently resembling the experimental one. However, the simulation for the P_2H_3 spin system was not nearly as satisfactory as for the $[\mathbf{2a}]^+$ homologue. An unrestricted full parameter optimization resulted in too broad lateral features and a too sharp central one, compared to the experimental spectrum (Figure 4), for a broadening factor of 2.07 G. An artificial reduction of the line broadening parameter to 1.4 G allows a perfect match of the two lateral features of the triplet, but the central feature becomes too sharp

relative to the experiment. This may indicate a dynamic exchange process on the EPR time scale. Indeed, virtual triplets displaying artificially broadened central features are commonly found in the NMR spectra of diamagnetic compounds featuring suitable site exchange phenomena, such as the X signal for an ABX system where sites A and B are near the fast exchange limit.^[40, 41] A rapid hydride scrambling process takes place for **[2a]⁺** (symmetric EPR coupling pattern, inequivalent hydride positions by X-ray crystallography), as well as for the neutral precursors (*vide supra*) and for the related $[\text{Cp}^*\text{Mo}(\text{dppe})\text{H}_3]^{n+}$ ($n = 0, 1$) complexes.^[9] This exchange is possibly slower for the more encumbered (C_5HiPr_4) derivative, causing the observed lineshape effect. It is interesting to note that the exchange rates are similar for the neutral precursors (slightly smaller for **2a**), whereas the exchange process appears faster in **2a⁺** than in **2b⁺**.

The next peculiar feature of the EPR spectrum of **[2b]⁺** is a much lower value shown by a_{P} and a_{H} (namely $a_{\text{P}} = 6.2$ G; $a_{\text{H}} = 1.7$ G; $a_{\text{Mo}} = 29.4$ G) relative to both **[2a]⁺** ($a_{\text{P}} = 36.2$ G, $a_{\text{H}} = 11.4$ G and $a_{\text{Mo}} = 30.8$ G)^[21] and $[\text{Cp}^*\text{Mo}(\text{dppe})\text{H}_3]^+$ ($a_{\text{P}} = 29.8$ G; $a_{\text{H}} = 11.8$ G).^[9] The cause of this phenomenon is not quite clear, but the different coupling values suggest that **[2b]⁺** adopts a different geometry relative to that of **[2a]⁺**, possibly involving the complete collapse of two hydrides to a dihydrogen ligand. It is easy to imagine how the greater bulk of the substituted cyclopentadienyl ring in **[2b]⁺** might force the two H atoms closer together. This phenomenon may well be related to the slower hydride mutual exchange, as well as to our inability to isolate the compound. Related to this point, we recall that the tetrahydride protonation product is stable in the case of **3a** but decomposes in the case of **3b**, although the same system **4a,b** is obtained in MeCN. Thus, we speculate that the extreme bulk of the C_5HiPr_4 ligand has the effect of pushing out an H_2 ligand from both systems **3b** and **[2b]⁺**.

(d) Oxidatively induced H₂ reductive elimination

Although compound [2a]⁺PF₆⁻ is quite stable as a crystallized solid and in THF solution at low temperatures, it slowly decomposed at T > 0°C, as indicated by a color change from orange to green. Well formed green crystals were obtained by slow crystallization from THF/pentane at -20°C. This product appeared thermally stable with no noticeable change over time in the solid state and in THF solution at room temperature. X-ray diffraction analysis revealed the identity of the compound as [(1,2,4-C₅H₂tBu₃)MoH(PMe₃)₂]⁺PF₆⁻, **5a**. A view of the structure is presented in our previous communication,^[21] while selected bonding parameters are reported in Table 1. Therefore, the compound derives from its precursor [2a]⁺PF₆⁻ by H₂ elimination, see Scheme 4.



Scheme 4

Although the quality of the data set allowed the identification of a single hydride ligand with a high level of confidence (see Experimental section), the question of the possible presence of additional hydride ligands in the structure of compound **5a** has been considered carefully, since hydrogen atoms may be difficult to locate from X-ray diffraction data. Possibilities include the presence of one, two or three additional hydride ligands, giving a 16-electron dihydride, a 17-electron trihydride (a stereoisomer of the precursor [2a]⁺), and an 18-electron tetrahydride cation (i.e. complex **3a**), as well as a dihydrogen ligand, yielding a nonclassical tautomer of [2a]⁺. The color of **5a** relative to [2a]⁺PF₆⁻ excludes an isomeric form of [2a]⁺ and also the tetrahydride formulation, although the bond distances and angles related to the heavy atoms in the cation of **5a**, see Table 1, are not too different from those observed for compound **3a**.

The ^1H NMR spectrum of the isolated solid only revealed the resonances of the tetrahydride complex **3a**, indicating that this compound is a decomposition by-product (the solid was a mixture of well formed crystals and a powder). Complex **3a** certainly arises from the transfer of a proton from acidic $[\mathbf{2a}]^+$ to residual **2a**, similarly to what occurs for the $\text{Cp}^*\text{Mo}(\text{dppe})\text{H}_3$ analogue.^[16] A solid sample of the isolated compound showed bulk paramagnetism, however a reliable value for the magnetic moment could not be obtained, given the impure nature of the sample. ^1H NMR monitoring of the decomposition reaction also showed the formation of **3a**, in addition to the formation of H_2 .

Positive identification of the green decomposition product as a 15-electron species comes from EPR spectroscopy. As detailed in the communication,^[21] the solid sample shows features consistent with a spin quartet ground state at the liquid He temperature (Figure 5a): g_x and g_y at 3.74 and 3.45 ($\pm 1/2$ transition), plus a weak feature (g_z for the forbidden $\pm 3/2$ transition) at 5.33. The $g = 3.74$ peak appears to display a fine structure, possibly due to coupling to the two equivalent P nuclei. The g_z component of the $\pm 1/2$ transition is not visible because it is overshadowed by stronger resonances in the $g = 2$ region (shown in Figure 5b). The resonance observed at $g = 2.009$ for the polycrystalline sample is very close to the position observed at higher temperature for the precursor complex $[\mathbf{2a}]^+$ and is therefore attributed to a residual amount of this material, which had co-crystallized with the H_2 elimination product **5a** (see Experimental section).

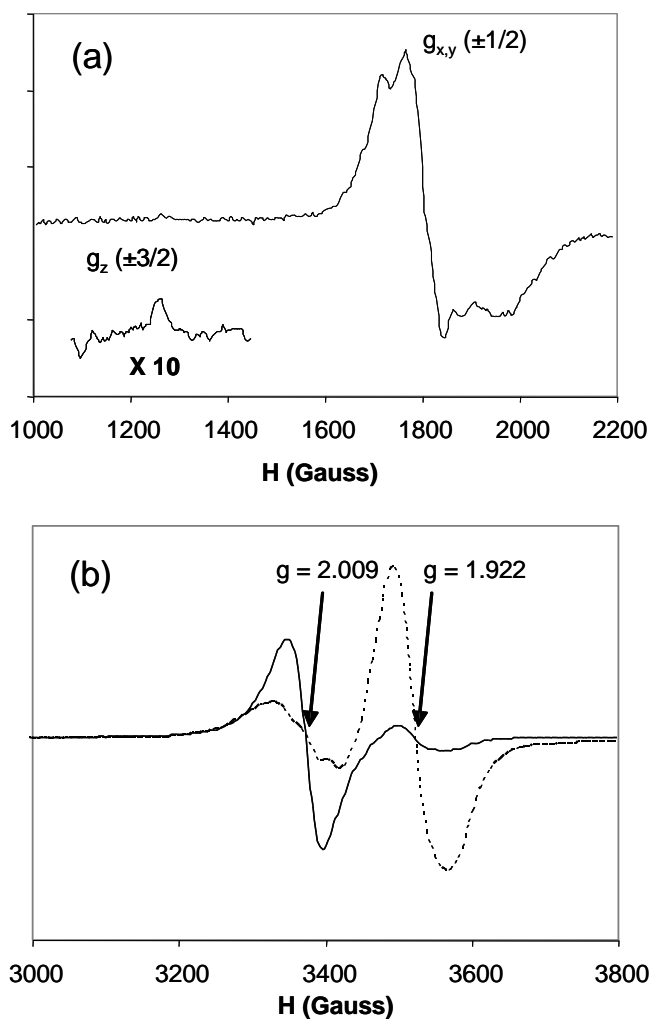


Figure 5. Liquid He EPR spectrum of compound **5a**: (a) polycrystalline sample in the $g = 4$ - 6 region; (b) polycrystalline sample (solid line) and frozen THF glass (dashed line) in the $g = 2$ region.

Solutions of compound **5a** in THF were EPR silent at room temperature and showed only a weak resonance at the liquid nitrogen temperature. On the other hand, they show an intense band at $g = 1.922$ at the liquid He temperature. The two resonances at $g = 2.009$ and 1.922 are visible for both polycrystalline and THF solution samples, but their relative intensity is opposite. The latter must belong to another $S = \frac{1}{2}$ complex and we therefore assign it to the THF adduct, $[(1,2,4\text{-C}_5\text{H}_2\text{tBu}_3)\text{Mo}(\text{PMe}_3)_2(\text{THF})\text{H}]^+$. Its presence for the polycrystalline sample, which had been obtained by crystallization from THF (see Experimental section), represents evidence of solution equilibrium between the solvent-free,

15-electron, spin quartet monohydride complex and a spin doublet solvent adduct. The compound crystallizes preferentially in the solvent-free form, but the THF adduct also appears to exist in the solid state. Additional evidence for this equilibrium will be provided by the electrochemical analysis (*vide infra*).

As stated in the Introduction, we previously reported the first unambiguous oxidative induced reductive elimination of H₂ from the one-electron oxidation of complex Cp*Mo(dppe)H₃. However, the elimination product could not be crystallized and was only characterized in solution as the 17-electron solvent adduct [Cp*Mo(dppe)(solv)H]⁺ by EPR spectroscopy (solv = THF, CH₂Cl₂)^[9] and by electrochemistry (solv = MeCN).^[16] The steric bulk of the PMe₃ and 1,2,4-C₅H₂tBu₃ ligands, in combination with the electron pairing stabilization provided by the spin quartet state,^[42, 43] accounts for the absence of solvent coordination to complex **5a**. The oxidatively induced reductive elimination of compounds containing two one-electron ligands {M(X)(Y), leading to the elimination of X-Y} has previously been demonstrated for dialkyl complexes {M(R)₂} to give the alkane coupling product R-R^[18, 44-50] and for alkyl-hydride complexes {M(R)(H)} to give the corresponding alkane R-H,^[18, 47] plus products originating from {M}⁺. To the best of our knowledge, the 15-electron {M}⁺ product was not isolated and characterized in any of those studies. For X = Y = H, as stated in the Introduction, oxidation often results in dihydrogen evolution but the multitude of decomposition pathways of the intermediate oxidized polyhydride complexes often obscure the clean identification of the oxidatively induced reductive elimination pathway. Therefore, the present investigation illustrates the first well defined example of an oxidatively induced reductive elimination of H₂, through the full characterization of starting and end product of the H₂ elimination process.

Since the greater bulk of the C₅H₇Pr₄ ring should cause an even more favorable H₂ elimination process, the decomposition of the less thermally stable [**2b**]⁺ would be expected to

lead to another 15-electron monohydride species, **5b**, analogous to **5a**. Upon warming to room temperature, orange solutions of **[2b]⁺** change color to blue, but the transformation is accompanied by the development of new EPR signals indicative of other $S = \frac{1}{2}$ species, which replaced the signal of the cationic trihydride complex. Thus, this decomposition is less well behaved than that of **[2a]⁺**, which led to an EPR silent solution (at room temperature). We cannot exclude the presence of species **5b** in this solution, but attempts to crystallize one or more of the decomposition products from this solution were unsuccessful.

(e) Electrochemical studies

Both compounds **2** exhibit a reversible one-electron oxidation in both THF and MeCN at the usual scan rates. The measured $E_{1/2}$ values for **2a** and **2b** are very similar (**2a**: -0.93 V in MeCN, -0.89 V in THF; **2b**: -0.95 V in MeCN, -0.88 in THF vs. the ferrocene standard). These potentials are slightly more negative than those measured for the related Cp*Mo(dppe)H₃ compound (-0.85 V in MeCN and -0.73 V in THF)^[9] in agreement with the greater electron donating power of the coordination sphere. While the process is reversible in THF for scan rates as low as 10 mV s⁻¹ for both compounds, the back reduction wave loses intensity relative to the oxidation wave at slow scan rates in MeCN. A figure is provided in the Supporting Information.

The cyclic voltammetry of compounds **2a** and **2b** has been investigated in MeCN and THF at variable scan rates and different potential ranges. The observed behavior is closely related to that of complex Cp*Mo(dppe)H₃,^[9, 16] a detailed study of which revealed three simultaneous decomposition pathways for the one-electron oxidation product, [Cp*Mo(dppe)H₃]⁺: deprotonation, disproportionation and H₂ elimination. Each pathway could be independently quantified (e.g. $k_{deprot} = 2.8(2) \cdot 10^2 \text{ s}^{-1} \text{ M}^{-1}$, $k_{disp} = 3.98(9) \cdot 10^3 \text{ s}^{-1} \text{ M}^{-1}$ and $k_{elim} = 2.0(4) \cdot 10^{-2} \text{ s}^{-1} \text{ M}^{-1}$ in MeCN).^[9, 16] For complexes **2a** and **2b**, we did not carry out a

thorough quantitative study. Rather, we focused only the voltammetric features that could provide additional information about the H₂ elimination pathway.

All three decomposition pathways of [Cp*Mo(dppe)H₃]⁺ have an associative character: disproportionation is initiated by solvent coordination to the 17-electron [Cp*Mo(dppe)H(H₂)]⁺ isomer; deprotonation needs the involvement of a molecule of neutral, 18-electron Cp*Mo(dppe)H₃; and H₂ elimination follows initial MeCN coordination.^[16] Indeed, the H₂ elimination is much slower in THF ($k_{elim} = 2.2(2) \cdot 10^{-5} \text{ s}^{-1} \text{ M}^{-1}$; measured independently by decay of the EPR signal),^[9] with no visible consequence on the cyclic voltammetric behavior in this solvent. Since compounds **2a** and **2b** have a more crowded coordination sphere than Cp*Mo(dppe)H₃, the above three pathways should be slower. However, whereas both disproportionation and deprotonation pathways demand a rate determining associative step, the H₂ elimination may also occur dissociatively, in which case the greater ligand steric pressure should accelerate it. We remind here that compound **5a** is the *stable* product of H₂ dissociation from [**2a**]⁺, although equilibrium amounts of the solvent adduct are present in THF (see EPR characterization above). This suggests a dissociative H₂ elimination process in THF but does not exclude an associative process in MeCN.

A two-scan cyclic voltammogram of **2a** at a scan rate of 5 V s⁻¹ is shown in Figure 6. When the scan is reversed at 0.7 V (vs. the reference Ag/AgCl electron, *i.e.* 0.27 V vs. ferrocene), only an additional oxidation peak **B** at -0.10 V (-0.05 V for **2b**) is observed in the voltammogram, in addition to the reversible one-electron oxidation of **2a** at A/A'. There is no return wave associated to this peak, indicating that the generated species decomposes rapidly. Note that the voltammogram does not change significantly in the second scan. When the potential sweep is switched at a higher potential, on the other hand, a third oxidation process **D**, also irreversible, appears at ca. 0.8 V. Following the first potential sweep reversal, a new reversible process at C/C' becomes visible at E_{1/2} = -0.15 V (-0.10 V for **2b**). Oxidation peak

C overlaps with peak **B** in the second scan. The behavior of compound **2b** is very similar to that of **2a**. The **C/C'** process shows a reduced reversibility for compound **2b**. Voltammograms of **2a** and **2b** at variable scan rates are available in the Supporting Information.

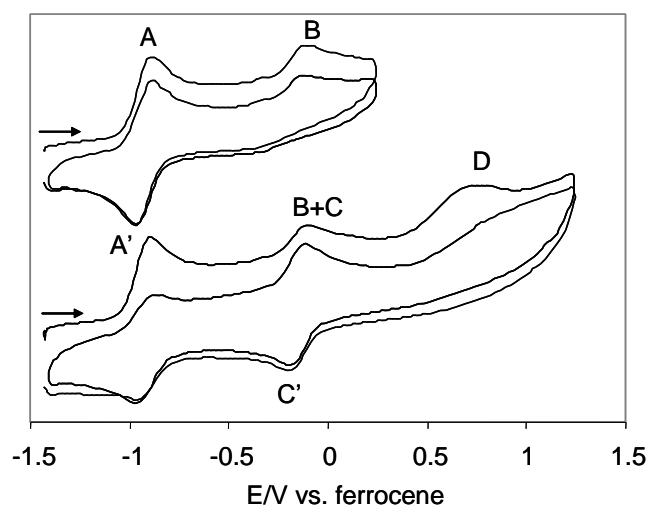
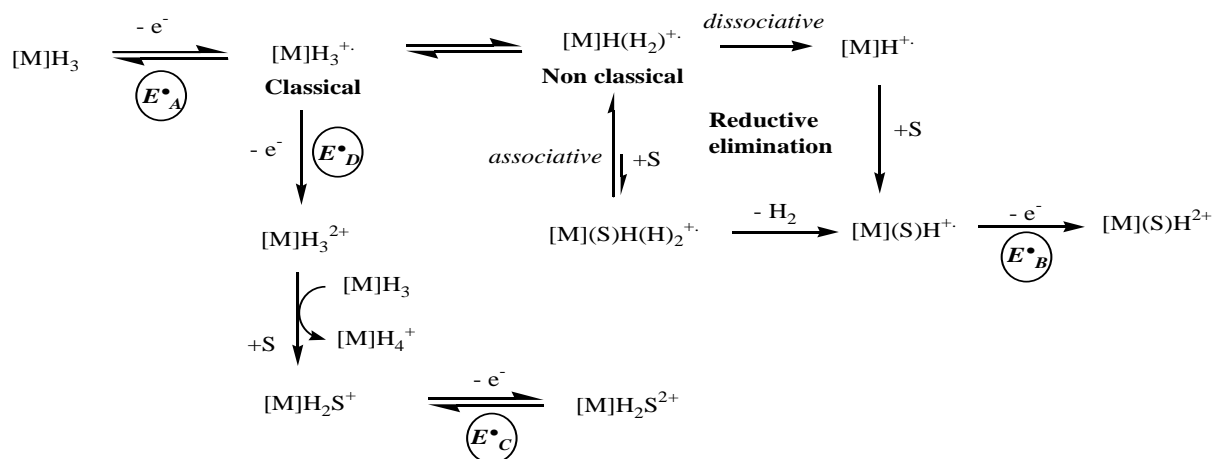


Figure 6. Two-scan cyclic voltammograms of compound **2a** in MeCN. Scan rate = 5000 mV s^{-1} .

According to the previous study, the above observations are interpreted as follows, see Scheme 5. The 17-electron $[\text{M}]\text{H}_3^{+}$ complex produced at **A** yields (via the nonclassical isomer $[\text{M}]\text{H}(\text{H}_2)^{+}$) complex $[\text{M}]\text{H}(\text{MeCN})^{+}$, which is responsible for the oxidation peak **B**. The complete lack of reversibility for the latter is due to the immediate saturation by solvent coordination, to afford the 18-electron $[\text{M}]\text{H}(\text{MeCN})_2^{2+}$. On the other hand, subsequent oxidation of $[\text{M}]\text{H}_3^{+}$ at **D** leads to the 16-electron $[\text{M}]\text{H}_3^{2+}$, which is immediately followed by proton transfer to the starting material $[\text{M}]\text{H}_3$ with formation of $[\text{M}]\text{H}_4^+$ (redox inactive) and $[\text{M}]\text{H}_2(\text{MeCN})^+$. The latter is responsible for the reversible process **C/C'**. A deeper analysis of these processes and complimentary investigations confirming their assignment were carried out during the previous study.^[16] The two anodic waves of peaks **B** and **C** accidentally overlap for $[\text{M}] = (1,2,4\text{-C}_5\text{H}_2\text{tBu}_3)\text{Mo}(\text{PMe}_3)_2$, whereas they differ only slightly for $[\text{M}] = \text{Cp}^*\text{Mo}(\text{dppe})$ ($\Delta E = 0.14 \text{ V}$).^[16] The essentially identical potentials measured for 17-electron

$[M]H(MeCN)^{+\bullet}$ and 18-electron $[M]H_2(MeCN)^+$ agree with a high covalent nature for the Mo-H bond.



Scheme 5

The essential point is that peak **B** is observed even at the highest scan speeds (up to 5 V s⁻¹), whereas the same process for system Cp*Mo(dppe)H₃ became observable only at $v < 0.6$ V s⁻¹ in neat MeCN. This illustrates that the H₂ elimination process is fast for systems **[2a]**⁺ and **[2b]**⁺, faster than when [M] = Cp*Mo(dppe), thus strongly suggesting that it proceeds dissociatively.

The voltammograms of **2a** in THF, see Figure 7, show many similarities but also interesting differences with respect to the behavior of the same compound in MeCN and to that of compound Cp*Mo(dppe)H₃ in THF. Following the oxidation at **A**, the irreversible peak **B** and the second oxidation process **D** are observed like in MeCN. Transit over process **D** does not generate a reversible C/C' couple. Transit over process **B**, on the other hand, generates a weak and broad reduction peak **E** at ca. -1.9 V, while peak **A** loses reversibility. A full rationalization of all these observations is not possible, as many of the species

implicated in Scheme 5 may be unstable and evolve to other unknown products when $S = \text{THF}$. Whereas the potentials of peaks **A** and **D** are close to the values observed in MeCN, peak **B** occurs at $E_{p,a}$ ca. 0.25 V in THF (vs. -0.18 V in MeCN). The more positive potential in THF may be related to a reduced donating power of THF relative to MeCN and/or to a more extensive solvent dissociation equilibrium established by the THF adduct with the 15-electron complex. Indeed, the presence of this equilibrium has been evidenced by the EPR study (see above). The most interesting feature, however, is the fact that compound **2a** shows peak **B** also in THF, whereas compound $\text{Cp}^*\text{Mo}(\text{dppe})\text{H}_3$ only shows it in MeCN.^[16] This is consistent with a dissociative mechanism for the H_2 substitution in $[\mathbf{2a}]^+$, in which case the rate should be essentially solvent independent. Indeed, peak **B** is observable in THF even at the fast scan rates (1 V s^{-1}).

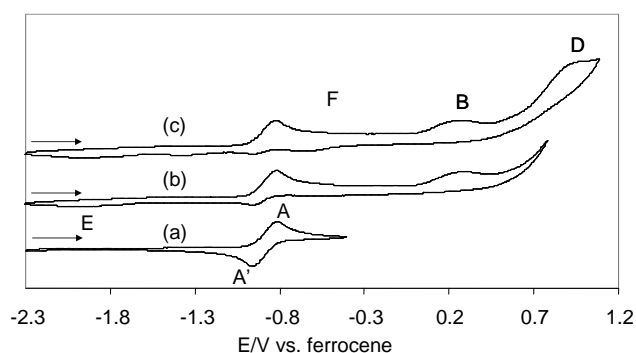


Figure 7. Cyclic voltammograms of compound **2a** in THF with different switching potentials. Scan rate = 200 mV s^{-1} .

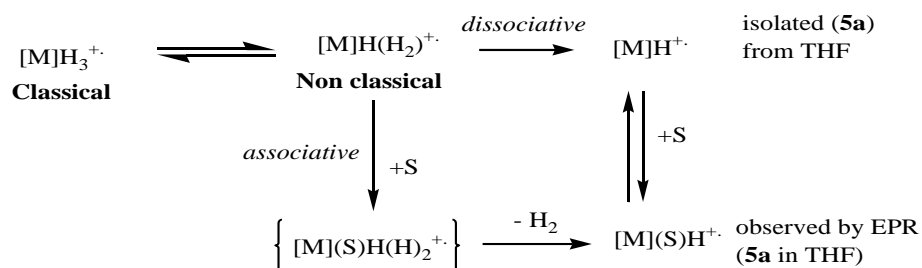
The behavior of **2b** in THF shows similarities to that of **2a** (see figure in the Supporting Information). Notably, a peak corresponding to process **B** is again present ($E_{p,a} = 0.2 \text{ V}$ vs. ferrocene). The behavior at higher potential, however, is more complex and not fully understood. It is possible that only a fraction of $[\mathbf{2b}]^+$ undergoes H_2 elimination, in competition with other decomposition processes, in the THF solvent. This seems to be suggested also by the EPR monitoring of this decomposition (*vide supra*). It seems clear,

however, that the first decomposition mode (H_2 elimination to afford a 15-electron derivative, possibly in equilibrium with a 17-electron THF adduct) is also established by this system.

Conclusion

We have shown that the combination of greater ligand donor power and greater steric bulk in the coordination sphere of half sandwich Mo^{IV} trihydride complexes stabilizes the 17-electron products of one-electron oxidation. Complex $[(1,2,4\text{-C}_5\text{H}_2\text{tBu}_3)\text{Mo}(\text{PMe}_3)_2\text{H}_3]^+$ is sufficiently stable to be crystallized and structurally characterized. Its geometry is very close to that of the neutral precursor, except that the separation between two hydride ligands is shorter suggesting the presence of a stretched dihydrogen ligand (or compressed MH_2 moiety). To the best of our knowledge, this is the first time that such evidence has been obtained for a paramagnetic polyhydride system. The steric control in this system, however, is rather subtle: on going from the 1,2,4- $\text{C}_5\text{H}_2\text{tBu}_3$ system to the more encumbered C_5HiPr_4 system, the paramagnetic trihydride product becomes less stable and could not be isolated. The C_5HiPr_4 ligand might impose such steric pressure to the MoH_3 system as to force a stronger interaction between two hydride ligands and a more favorable expulsion of H_2 . This also appears true for the tetrahydrido protonation product (**3a** vs. **3b**). A peculiar difference between the ground state properties of $[\mathbf{2a}]^+$ and $[\mathbf{2b}]^+$ has been evidenced by EPR spectroscopy (Figure 4). The present investigation has also revealed a dissociative pathway for H_2 substitution by a solvent molecule in the paramagnetic system. The oxidative behavior of the half-sandwich Mo trihydride system is summarized in Scheme 6: H_2 substitution by MeCN on $[\text{Mo}]\text{H}_3^+$ is associative for $[\text{Mo}] = \text{Cp}^*\text{Mo}(\text{dppe})$ and dissociative for $\text{Cp}^\# \text{Mo}(\text{PMe}_3)_2$; an equilibrium has been established by EPR spectroscopy for the latter system between the 15-electron species (complex **5a**) and its solvent adduct in THF, whereas

no evidence was previously obtained for a 15-electron species in the Cp*Mo(dppe) case. The dissociative product has in fact been isolated and structurally characterized, providing the first well characterized example of an oxidatively induced reductive elimination of H₂ from a polyhydride compound.



Scheme 6

Experimental Section

General procedures. All operations were carried out under an atmosphere of argon using standard Schlenk line and glove box techniques. Solvents were dehydrated (CH₂Cl₂: CaH₂; THF, toluene, sodium benzophenone ketyl) and distilled under dinitrogen prior to use. Mo(CO)₆ and PMe₃ (1 M solution in THF) were purchased from Aldrich and used as received. Compounds 1,2,4-tri(*tert*-butyl)- and tetra(*iso*-propyl)-cyclopentadiene (as isomer mixtures) were prepared by literature methods^[51, 52] and converted to their corresponding sodium salts by reaction with NaNH₂.

(b) Measurements. NMR measurements were carried out on either a Bruker AC 200 or a Bruker AMX250 spectrometer and calibrated with the residual solvent resonances (¹H) or with external 85% H₃PO₄ (³¹P). The lineshape analyses for the dynamic processes were carried out by simulation with DNMR3, which is incorporated into the freely available SpinWorks program.^[53] EPR spectra were measured on a Elexsys E500 BRUKER

spectrometer equipped with both a frequencymeter and gaussmeter. The spectrometer frequency was calibrated with diphenylpicrylhydrazyl (DPPH, $g = 2.0037$). EPR spectra simulations and fittings were carried out with the freely available WinSim program.^[54] Cyclic voltammograms were recorded with an EG&G 362 potentiostat connected to a Macintosh computer through MacLab hardware/software. The electrochemical cell was fitted with an Ag-AgCl reference electrode, a platinum disk working electrode and a platinum wire counter-electrode. $[\text{Bu}_4\text{N}]\text{PF}_6$ (ca. 0.1 M) was used as supporting electrolyte. The ferrocene standard had a potential of 0.43 V in MeCN and 0.62 V in THF under our experimental conditions.

Synthesis of (1,2,4- $\text{C}_5\text{H}_2\text{tBu}_3$) $\text{Mo}(\text{CO})_3\text{CH}_3$. A solution of $\text{Na}(1,2,4\text{-C}_5\text{H}_2\text{tBu}_3)$ (1.95 g, 8.3 mmol) in THF (20 mL) was transferred into a suspension of $\text{Mo}(\text{CO})_6$ (2.20 g, 8.3 mmol) in THF (15 mL). The mixture was heated to reflux for 15 h, during which time a colour change from pale yellow to dark red was observed. The mixture was then cooled and CH_3I (1 mL, 16 mmol) was added via syringe, causing an immediate colour change to bright yellow. Subsequently, the mixture was heated to reflux for 2 h; following which it was cooled and the solvents evaporated. The residue was then extracted with pentane (100 mL) and the pentane solution evaporated to yield $(1,2,4\text{-C}_5\text{H}_2\text{tBu}_3)\text{Mo}(\text{CO})_3\text{CH}_3$ as a yellow solid. Yield = 2.642 g; 74 %. IR (CH_2Cl_2): 2005, 1918 cm^{-1} (ν_{CO}).

Synthesis of ($\text{C}_5\text{H}_i\text{Pr}_4$) $\text{Mo}(\text{CO})_3\text{CH}_3$. A solution of $\text{Na}(\text{C}_5\text{H}_i\text{Pr}_4)$ (2.82 g, 11.0 mmol) in THF (25 mL) was transferred into a suspension of $\text{Mo}(\text{CO})_6$ (2.88 g, 10.9 mmol) in THF (20 mL). The mixture was heated to reflux for 16 h, during which time a colour change from pale yellow to dark red was observed. The mixture was then cooled and CH_3I (1.5 mL, 24 mmol) was added via syringe, causing an immediate colour change to bright yellow. Subsequently, the mixture was heated to reflux for 2 h; following which it was cooled and the solvents evaporated. The residue was then extracted with pentane and the pentane solution evaporated to yield $(1,2,4\text{-C}_5\text{H}_2\text{tBu}_3)\text{Mo}(\text{CO})_3\text{CH}_3$ as a yellow solid. Yield = 3.739 g; 80 %.

The compound was used directly for the synthesis of $(C_5H_9Pr_4)MoCl_4$ (see below), without characterisation.

Synthesis of $(1,2,4-C_5H_2tBu_3)MoCl_4$, **1a.** A solution of $PhICl_2$ (5 g, 38.2 mmol) in dichloromethane (20 mL) was transferred slowly into a solution of $(1,2,4-C_5H_2tBu_3)Mo(CO)_3CH_3$ (2.64 g, 6.2 mmol) in dichloromethane (15 mL). The mixture was heated to reflux for 3 h during which time a colour change from brown to indigo was observed. Solvents were then concentrated to ca. 3 mL and the resulting suspension was filtered to give a purple solid, which was washed with portions of pentane (5 x 50 mL) and then dried under reduced pressure to give $(1,2,4-C_5H_2tBu_3)MoCl_4$, **1a**, as a purple solid. Yield = 2.32 g, 79 %. EPR: $g = 1.992$, $a_{Mo} = 38.8$ G.

Synthesis of $(C_5H_9Pr_4)MoCl_4$, **1b.** $PhICl_2$ (6.87 g, 52.50 mmol) dissolved in dichloromethane (20 mL) was added dropwise to a solution of $(C_5H_9Pr_4)MoCO_3CH_3$ (6.85 g, 15.98 mmol) in dichloromethane (20 mL). The solution was heated to reflux for 3 h, during which time a colour change from brown to indigo was observed. Solvents were then concentrated to ca. 4 mL and the resulting suspension was filtered. The solid was washed with portions of pentane (5 x 20 mL) and dried under reduced pressure to give $(C_5H_9Pr_4)MoCl_4$, **1b**, as an indigo solid. Yield = 5.27 g, 70 %.

Synthesis of $(1,2,4-C_5H_2tBu_3)Mo(PMe_3)_2H_3$, **2a.** Compound **1a** (1415 mg, 3.00 mmol) was dissolved in tetrahydrofuran (20 mL) and a solution of trimethylphosphine in tetrahydrofuran (1 M, 8 mL, 8 mmol) was added. The mixture was stirred for 30 min, and then a suspension of lithium tetrahydroaluminate (ca. 650 mg) in tetrahydrofuran (40 mL) was carefully added. Gas evolution was observed during the addition. The mixture was stirred for 5 h then methanol (ca. 6 mL) was added dropwise causing vigorous gas evolution. The resulting suspension was stirred for 1 h and vacuum-dried; the residue was then extracted with diethyl ether (ca. 150 mL) and filtered through Celite 545. The final solution was vacuum-

dried, and the residue washed three times with methanol (6, 4 and 4 mL) and dried *in vacuo*. The product **2a** was obtained as a pale yellow solid. Yield: 727 mg (50 %). Anal. Calcd. for $C_{23}H_{50}MoP_2$: C, 57.01; H, 10.40. Found: C, 56.48; H, 10.88. 1H NMR (C_6D_6): δ -5.20 (t, J = 51.0 Hz, 3 H, Mo-*H*), 1.37 (s, 9 H, tBu), 1.49 (br, 18 H, $P(CH_3)_3$), 1.58 (s, 18 H, 2 x tBu), 4.86 (s, 2 H, $C_5H_2^tBu_3$). $^{31}P\{^1H\}$ NMR (C_6D_6): δ 17.9 (s). A single crystal for the X-ray analysis was obtained by slow diffusion of a MeOH layer into a pentane solution at 5°C.

Synthesis of $(C_5H_iPr_4)Mo(PMe_3)_2H_3$, **2b.** Compound **1b** (890 mg, 1.89 mmol) was dissolved in tetrahydrofuran (20 mL), and a solution of trimethylphosphine in tetrahydrofuran (1 M, 5 mL, 5 mmol) was added. The mixture was stirred for 20 min and a suspension of lithium tetrahydroaluminate (*ca.* 500 mg) in tetrahydrofuran (40 mL) was carefully added. Gas evolution was observed during the addition. The mixture was stirred for 6 h, after which methanol (*ca.* 5 mL) was added drop by drop. Vigorous gas evolution was observed at this point. The resulting suspension was stirred for 1 h and then vacuum-dried. The residue was extracted with diethyl ether (*ca.* 100 mL) and filtered through Celite 545. The final solution was vacuum-dried and the residue washed with portions of methanol (5, 3 and 3 mL) and dried *in vacuo*. The product **2b** was obtained as an orange-yellow solid. Yield: 449 mg (49 %). Anal. Calcd. for $C_{23}H_{50}MoP_2$: C, 57.01; H, 10.40. Found: C, 56.91; H, 11.10. 1H NMR (C_6D_6): δ -5.15 (t, J = 52.9 Hz, 3 H, Mo-*H*), 1.30 - 1.80 (42 H, $CH(CH_3)_2$, $P(CH_3)_3$), 2.79 (m, 2 H $CH(CH_3)_2$), 2.96 (m, 2 H $CH(CH_3)_2$), 4.72 (s, 1 H, $C_5H^iPr_4$). $^{31}P\{^1H\}$ NMR (C_6D_6): δ 17.3 (s). A single crystal for the X-ray analysis was obtained by diffusion of a MeCN layer onto a THF solution at room temperature.

Synthesis of $[(1,2,4-C_5H_2tBu_3)Mo(PMe_3)_2H_3]^+PF_6^-$, **2a $^+PF_6^-$.** A suspension of $[Fe(\eta^5-C_5H_5)_2]PF_6$ (32 mg, 0.10 mmol) in tetrahydrofuran (5 mL) was added dropwise to a cold solution (193 K) of compound **2a** (53 mg, 0.11 mmol) in tetrahydrofuran (5 mL). The solution color immediately changed from pale yellow to dark blue and, within a few minutes,

to orange. The reaction mixture was slowly warmed up to 253 K and then concentrated to *ca.* 1 mL. Addition of cold pentane (253 K, 10 mL) afforded a brown precipitate that was decanted and further washed with cold pentane (253 K, 3x10 mL) and finally vacuum-dried. The product **2a**⁺PF₆⁻ was obtained as a pale brown solid. Yield: 48 mg, 70 %. EPR (THF): *g* = 2.0185, *a_P* = 36.2 G, *a_H* = 11.4 G, *a_{Mo}* = 30.8 G. A single crystal for the X-ray analysis was obtained by diffusion of a pentane layer onto a THF solution at -80°C.

Synthesis of [(1,2,4-C₅H₂tBu₃)Mo(PMe₃)₂H₄]⁺BF₄⁻, **3a.** A solution of (*η*⁵-C₅H₂¹Bu₃)Mo(PMe₃)₂H₃ (**2a**, 40 mg, 0.08 mmol) in diethyl ether (4 mL) was cooled to -80°C. HBF₄ (54 % solution in diethyl ether, 22 μL, 0.16 mmol) was added via syringe. Within minutes, a white precipitate formed. A further portion of diethyl ether (2 mL) was added. The solvent was then decanted and the solid washed with portions of diethyl ether (5 x 3 mL) and dried under reduced pressure to yield **3a** as a white solid. Yield: 39 mg, 85 %. ³¹P{¹H} NMR (THF-*d*₈): δ 0.4 (s). ¹H NMR (THF-*d*₈): δ -4.20 (t, *J* = 53.4 Hz, 3 H, Mo-H), 1.38 (s, 9 H, ¹Bu), 1.46 (s, 18 H, 2 x ¹Bu), 1.78 (br, 18 H, P(CH₃)₃), 5.08 (s, 2 H, C₅H₂¹Bu₃). A single crystal for the X-ray analysis was obtained by diffusion of a diethyl ether layer onto a THF solution at room temperature.

Generation of [(1,2,4-C₅H₂tBu₃)Mo(PMe₃)₂(MeCN)H₂]⁺BF₄⁻, **4a.** [(1,2,4-C₅H₂tBu₃)Mo(PMe₃)₂H₄]⁺BF₄⁻ (**3a**, 10 mg, 0.018 mmol) was measured into an NMR tube and dissolved in CD₃CN. ¹H and ³¹P NMR spectra were recorded initially and again after 5 h. At this time, the resonances corresponding to **3a** were replaced by a new set of resonances, ascribed to [(1,2,4-C₅H₂tBu₃)Mo(PMe₃)₂H₂MeCN]⁺BF₄⁻, **4a**. ³¹P{¹H} NMR (CD₃CN): δ 1.85 (s). ³¹P{¹H sel. decoupler at 1.61 ppm} δ 1.88 (t, *J* = 52.85 Hz) ¹H NMR (CD₃CN, 298 K): δ 1.07 (9H, s, C(CH₃)₃), 1.42, (18H, s, 2 x C(CH₃)₃), 1.61 (18H, d, *J* = 8.7 Hz, P(CH₃)₃), 2.17 (3H, s, CH₃CN) 4.59 (m, 2H, C₅H₂¹Bu₄). ¹H NMR (CD₃CN, 233 K): δ -6.77 (1H, t, *J_{P-H}* = 40.0 Hz, Mo-H), -0.27 (1H, t, *J_{P-H}* = 80 Hz, Mo-H), 1.03 (9H, s, C(CH₃)₃), 1.38 (18H, s,

$C(CH_3)_3$), 1.58 (18H, d, $J_{P-H} = 10$ Hz, $P(CH_3)_3$), 2.40 (3H, s, CH_3CN), 4.58 (2H, m, $C_5H_2^iBu_3$).

Generation of $[(C_5H^iPr_4)Mo(PMe_3)_2H_2(MeCN)]^+BF_4^-$, **4b.** A solution of HBF_4 (54 % in diethyl ether, 7.4 μ L, 0.05 mmol) was added to a solution of $(\eta^5-C_5H^iPr_4)MoH_3(PMe_3)_2$ (26 mg, 0.05 mmol) in thf (1 mL) and MeCN (1 mL) at -80 °C. A color change from yellow to orange was observed immediately. Solvents were concentrated to 1 mL and diethyl ether (1 mL) was added to aid the precipitation of a yellow solid. The solution was filtered and the solid washed with portions of diethyl ether (5 x 2 mL) and dried under reduced pressure to give **4b** as a yellow solid. $^{31}P\{^1H\}$ NMR (acetone- d_6): δ 4.66 (s). $^{31}P\{^1H$ sel. decoupler at 1.68 ppm} δ 4.68 (t, $J = 54.7$ Hz) 1H NMR (acetone- d_6 , 298 K): δ -2.5 (br, 2H, Mo- H), 1.18 (12H, d, $J = 8.2$ Hz, $CH(CH_3)_2$), 1.31, (12H, d, $J = 8.6$ Hz, $CH(CH_3)_2$), 1.69 (18H, d, $P(CH_3)_3$), 2.71 (7H, m, $CH(CH_3)_2$, CH_3CN) 4.92 (s, 1H, $C_5H^iPr_4$). 1H NMR (acetone- d_6 , 200 K): δ -5.27 (1H, td, $J_{P-H} = 32.5$ Hz, $J_{H-H} = 10$ Hz Mo- H), -0.13 (1H, ddd, $J_{P-H} = 47.5$, 33.75, $J_{H-H} = 10$ Hz, Mo- H), 1.07 (3H, d, $J = 6.8$ Hz, $CH(CH_3)_2$), 1.13 (3H, d, $J = 6.8$ Hz, $CH(CH_3)_2$), 1.18 – 1.23 (9H, 3 x d, $J = 7.3$, 6.9 Hz, $CH(CH_3)_2$), 1.29 (3H, d, $J = 7.3$ Hz, $CH(CH_3)_2$), 1.39 (6H, 2 x d, $J = 6.5$ Hz, $CH(CH_3)_2$), 1.65 (18H, 2 x d, $J_{P-H} = 8.0$ Hz, $P(CH_3)_3$), 2.53 (1H, m, $J = 6.8$ Hz, $CH(CH_3)_2$), 2.58 (1H, m, $J = 7.3$ Hz, $CH(CH_3)_2$), 2.71 (2H, 2 x $CH(CH_3)_2$, m, $J = 6.5$ Hz), 2.79 (3H, s, CH_3CN), 5.02 (1H, d, $J = 6$ Hz, $C_5H^iPr_4$).

Formation of $[(1,2,4-C_5H_2^iBu_3)Mo(PMe_3)_2H]^+PF_6^-$, **5.** A solution of compound **2a** $^+PF_6^-$ in THF was stored at -20 °C for 2 days, after which time a mixture of green and dark orange-red crystals had formed. One of the green crystals was used for the X-ray analysis. For the spectroscopic properties, see Results and Discussion.

Single crystal X-ray and neutron diffraction studies. A single crystal of each compound was mounted under inert perfluoropolyether at the tip of glass fibre and cooled in the cryostream of either an Oxford-Diffraction XCALIBUR CCD diffractometer for **2b**, **4a**

and **5a** or a Stoe IPDS diffractometer for **2a**, **2a⁺**. Data were collected using the monochromatic MoK α radiation ($\lambda = 0.71073$). The structures were solved by direct methods (SIR97)^[55] and refined by least-squares procedures on F^2 using SHELXL-97.^[56] All H atoms attached to carbon were introduced in calculation in idealised positions and treated as riding models. In compound **2a⁺**, there are two cations and anions in the asymmetric unit and all the *t*Bu groups of one of the cations are disordered over two positions. In structure **2a**, coordinates and U_{iso} for the hydrides, were fully refined whereas in **3a**, the coordinates of the hydrides were fully refined with an overall isotropic thermal parameter. In **2a⁺** and **5a**, the coordinates of the hydrides were fully refined with $U_{\text{iso}} = 1.2U_{\text{eq}}[\text{Mo}(\mathbf{2a}^+)]$ or $U_{\text{iso}} = 1.5U_{\text{eq}}[\text{Mo}(\mathbf{5a})]$. The disordered moieties were refined applying the restraints available within SHELXL97.^[56] Moreover, some residual electron density was difficult to model and therefore, the SQUEEZE function of PLATON^[57] was used to eliminate the contribution of the electron density in the solvent region from the intensity data, and the solvent-free model was employed for the final refinement. There are four cavities per unit cell and PLATON estimated that each cavity contains 32 electrons which could be attributed to a disordered THF molecules. The data collected for compound **2b** were of very low quality and although the structural model is mainly correct, it was not possible to locate any hydride ligand. The drawing of the molecules was realised with the help of ORTEP32.^[58] Crystal data and refinement parameters are shown in Table 2.

The neutron single-crystal diffraction study was performed using the time-of-flight Laue diffractometer SXD^[59] installed at the ISIS pulsed spallation source. SXD uses the white beam Laue technique and a stationary crystal combined with eleven highly pixellated area detectors covering around half a sphere around the sample. Thus, large volumes in reciprocal space can be collected in a single shot. A suitable single crystal of the complex (**2a**) was fixed to an Aluminum pin with thin strips of adhesive Al tape and mounted on a He closed-cycle

refrigerator and cooled slowly to 20K. The space group $P2_1/n$ was confirmed at 20K. No significant change in the crystal mosaic or splitting of the peak was observed during cooling. Further crystallographic data and experimental details are given in Table 2 and in the Supporting Information. The unit cell dimensions were precisely calculated, at the end of the data collection, from the positions of 60 reflections per each detector orientation. Data were collected at nine different orientations at 20(1) K for ca. 24 hour per orientation. The range of wavelengths used for the data collection was $0.37 < \lambda < 8.8 \text{ \AA}$, even though the bulk of the diffraction information is obtained from the wavelength range $0.5 < \lambda < 7.0 \text{ \AA}$. Data reduction and a Gaussian absorption correction were performed using the standard SXD procedure implemented in the SXD2001 software^[60] resulting in a total of 8686 reflections of which 3203 were unique. The starting structural model for the refinement was based on the atomic co-ordinates for the non hydrogen atoms taken from the X-ray structural determination. The structure was refined by full matrix least squares, minimising the function $[\sum w(F_o^2 - (1/k)F_c^2)^2]$ and using all independent data. During the refinement, the difference-Fourier maps clearly showed all H atoms of the ligands and the three hydrides. The final structure model included co-ordinates and anisotropic displacement parameters for all atoms. Upon convergence the final Fourier difference map showed no significant features. The coherent scattering amplitudes used were those tabulated by Rauch and Waschkowski.^[61] All calculations were carried out by using the PC version of the programs WINGX,^[62] SHELX-97^[56] and ORTEP.^[58]

Crystallographic data (excluding structure factors) have been deposited with the Cambridge Crystallographic Data Centre as supplementary publication no. CCDC 631893 - 631898. Copies of the data can be obtained free of charge on application to the Director, CCDC, 12 Union Road, Cambridge CB2 1EZ, UK (Fax: (+44) 1223-336-033; E-mail: deposit@ccdc.cam.ac.uk).

Acknowledgements

We thank the European Commission through the HYDROCHEM program (contract HPRN-CT-2002-00176) for support of this work. MB thanks the Spanish Ministerio de Educación y Ciencia for a post-doctoral fellowship.

Supporting Information available

Figures showing the structure of **2a** from the neutron diffraction experiment, the variable temperature $^{31}\text{P}\{^1\text{H}\}$ experiment for compound **2b**, and a variety of cyclic voltammograms for **2a** and **2b** at variable scan speed in MeCN and THF (5 pages).

References

- [1] G. W. Parshall, *Homogeneous Catalysis: The Applications and Chemistry of Catalysis by Soluble Transition Metal Complexes*, John Wiley and Sons, New York, **1980**.
- [2] A. Dedieu, *Transition Metal Hydrides*, VCH, New York, **1992**.
- [3] M. Peruzzini, R. Poli, *Recent Advances in Hydride Chemistry*, Elsevier, Amsterdam, **2001**.
- [4] R. Y. Igarashi, M. Laryukhin, P. C. Dos Santos, H.-I. Lee, D. R. Dean, L. C. Seefeldt, B. M. Hoffman, *J. Am. Chem. Soc.* **2005**, *127*, 6231-6241.
- [5] S. Foerster, M. Stein, M. Brecht, H. Ogata, Y. Higuchi, W. Lubitz, *J. Am. Chem. Soc.* **2003**, *125*, 83-93.
- [6] R. Mejia-Rodriguez, D. S. Chong, J. H. Reibenspies, M. P. Soriaga, M. Y. Darensbourg, *J. Am. Chem. Soc.* **2004**, *126*, 12004-12014.
- [7] O. B. Ryan, M. Tilset, V. D. Parker, *J. Am. Chem. Soc.* **1990**, *112*, 2618-2626.
- [8] K.-T. Smith, C. Rømming, M. Tilset, *J. Am. Chem. Soc.* **1993**, *115*, 8681-8689.
- [9] B. Pleune, D. Morales, R. Meunier-Prest, P. Richard, E. Collange, J. C. Fettinger, R. Poli, *J. Am. Chem. Soc.* **1999**, *121*, 2209-2225.
- [10] V. Skagestad, M. Tilset, *J. Am. Chem. Soc.* **1993**, *115*, 5077-5083.
- [11] R. Poli, in *Recent Advances in Hydride Chemistry* (Eds.: R. Poli, M. Peruzzini), Elsevier Science, Amsterdam, **2001**, pp. 139-188.
- [12] B. Pleune, R. Poli, J. C. Fettinger, *J. Am. Chem. Soc.* **1998**, *120*, 3257-3258.
- [13] E. A. Quadrelli, H.-B. Kraatz, R. Poli, *Inorg. Chem.* **1996**, *35*, 5154-5162.
- [14] J. C. Fettinger, H.-B. Kraatz, R. Poli, E. A. Quadrelli, R. C. Torralba, *Organometallics* **1998**, *17*, 5767-5775.
- [15] E. A. Quadrelli, R. Poli, *Organometallics* **1998**, *17*, 5776-5781.
- [16] R. Poli, M. Baya, R. Meunier-Prest, S. Raveau, *New J. Chem.* **2006**, *30*, 759 - 773.
- [17] A. A. Zlota, M. Tilset, K. G. Caulton, *Inorg. Chem.* **1993**, *32*, 3816-3821.
- [18] A. Pedersen, M. Tilset, *Organometallics* **1994**, *13*, 4887-4894.
- [19] M. T. Costello, R. A. Walton, *Inorg. Chem.* **1988**, *27*, 2563-2564.
- [20] K.-T. Smith, M. Tilset, R. Kuhlman, K. G. Caulton, *J. Am. Chem. Soc.* **1995**, *117*, 9473-9480.
- [21] M. Baya, J. Houghton, J.-C. Daran, R. Poli, *Angew. Chem., Int. Ed. Engl.* **2007**, *46*, 429-432.
- [22] R. C. Murray, L. Blum, A. H. Liu, R. R. Schrock, *Organometallics* **1985**, *4*, 953-954.
- [23] D. W. Keogh, R. Poli, in *Synthetic Methods of Organometallic and Inorganic Chemistry (Herrmann/Brauer)*, Vol. 8 (Ed.: W. A. Herrmann), Georg Thieme Verlag, Stuttgart, **1997**, p. 98.
- [24] J. H. Shin, G. Parkin, *Chem. Commun.* **1998**, 1273-1274.
- [25] J. C. Fettinger, B. Pleune, R. Poli, *J. Am. Chem. Soc.* **1996**, *118*, 4906-4907.
- [26] B. Pleune, R. Poli, J. C. Fettinger, *Organometallics* **1997**, *16*, 1581-1594.
- [27] H. Sakaba, T. Hirata, C. Kabuto, K. Kabuto, *Organometallics* **2006**, *25*, 5145-5150.
- [28] G. J. Kubas, *Metal Dihydrogen and σ -Bond Complexes*, Kluwer Academic/Plenum Press, New York, **2001**.
- [29] D. M. Heinekey, J. M. Millar, T. F. Koetzle, N. G. Payne, K. W. Zilm, *J. Am. Chem. Soc.* **1990**, *112*, 909-919.
- [30] J. A. K. Howard, O. Johnson, T. F. Koetzle, J. L. Spencer, *Inorg. Chem.* **1987**, *26*, 2930-2933.

- [31] J. A. K. Howard, S. A. Mason, O. Johnson, I. C. Diamond, S. Crennell, P. A. Keller, J. L. Spencer, *J. Chem. Soc., Chem. Comm.* **1988**, 1502-1503.
- [32] L. Brammer, J. A. K. Howard, O. Johnson, T. F. Koetzle, J. L. Spencer, A. M. Stringer, *J. Chem. Soc., Chem. Commun.* **1991**, 241-243.
- [33] T. Hasegawa, Z. Li, S. Parkin, H. Hope, R. K. McMullan, T. F. Koetzle, H. Taube, *J. Am. Chem. Soc.* **1994**, *116*, 4352-4356.
- [34] T. J. Johnson, A. Albinati, T. F. Koetzle, J. Ricci, O. Eisenstein, J. C. Huffman, K. G. Caulton, *Inorg. Chem.* **1994**, *33*, 4966-4976.
- [35] T. M. Cameron, C. G. Ortiz, I. Ghiviriga, K. A. Abboud, J. M. Boncella, *J. Am. Chem. Soc.* **2002**, *124*, 922-923.
- [36] R. Poli, *Organometallics* **1990**, *9*, 1892-1900.
- [37] F. Abugideiri, J. C. Fettinger, D. W. Keogh, R. Poli, *Organometallics* **1996**, *15*, 4407-4416.
- [38] T.-Y. Cheng, D. J. Szalda, J. Zhang, R. M. Bullock, *Inorg. Chem.* **2006**, *45*, 4712-4720.
- [39] D. M. Heinekey, A. Lledós, J. M. Lluch, *Chem. Soc. Rev.* **2004**, 175-182.
- [40] J. Sandström, *Dynamic NMR Spectroscopy*, Academic Press, London, **1982**.
- [41] G. Binsch, *J. Am. Chem. Soc.* **1969**, *91*, 1304-1309.
- [42] R. Poli, *Chem. Rev.* **1996**, *96*, 2135-2204.
- [43] R. Poli, *J. Organometal. Chem* **2004**, *689*, 4291-4304.
- [44] D. G. Morrell, J. K. Kochi, *J. Am. Chem. Soc.* **1975**, *97*, 7262-7270.
- [45] T. T. Tsou, J. K. Kochi, *J. Am. Chem. Soc.* **1978**, *100*, 1634-1635.
- [46] W. Lau, J. C. Huffman, J. K. Kochi, *Organometallics* **1982**, *1*, 155-169.
- [47] A. Pedersen, M. Tilset, *Organometallics* **1993**, *12*, 56-64.
- [48] P. Diversi, S. Iaconi, G. Ingrosso, F. Laschi, A. Lucherini, C. Pinzino, G. Uccello-Barretta, P. Zanella, *Organometallics* **1995**, *14*, 3275-3287.
- [49] E. Fooladi, M. Tilset, *Inorg. Chem.* **1997**, *36*, 6021-6027.
- [50] E. Fooladi, T. Graham, M. L. Turner, B. Dalhus, P. M. Maitlis, M. Tilset, *J. Chem. Soc., Dalton Trans.* **2002**, 975-982.
- [51] H. Sitzmann, *J. Organometal. Chem.* **1988**, *354*, 203-214.
- [52] H. Sitzmann, *Z. Naturforsch.* **1989**, *44b*, 1293-1297.
- [53] K. Marat, *SpinWorks Version 2.5.4*, **2006**.
- [54] D. R. Duling, *P.E.S.T.*, v. 0.96, National Institute of Environmental Health Sciences, Research Triangle Park, NC, **1996**.
- [55] A. Altomare, M. Burla, M. Camalli, G. Cascarano, C. Giacovazzo, A. Guagliardi, A. Moliterni, G. Polidori, R. Spagna, *J. Appl. Cryst.* **1999**, *32*, 115-119.
- [56] G. M. Sheldrick, *SHELXL97. Program for Crystal Structure refinement*, University of Göttingen, Göttingen, Germany, **1997**.
- [57] A. L. Spek, *J. Appl. Cryst.* **2003**, *36*, 7-13.
- [58] L. J. Farrugia, *J. Appl. Crystallogr.* **1997**, *32*, 565.
- [59] D. A. Keen, M. J. Gutmann, C. C. Wilson, *J. Appl. Cryst.* **2006**, *39*, 714.
- [60] M. J. Gutmann, ISIS Facility, Rutherford Appleton Laboratory, U.K., **2006**.
- [61] H. Rauch, W. Waschkowski, in *Neutron Data Booklet* (Eds.: A. J. Dianoux, G. Lander), Institut Laue-Langevin: Grenoble, **2002**, pp. 1.1-1.
- [62] L. J. Farrugia, *J. Appl. Crystallogr.* **1999**, *32*, 837-838.

Table 1. Selected bond distances (Å) and angles (°) for all structurally characterized complexes

	2a		2b	3a	2a⁺		5a
	X-ray	neutron	X-ray	X-ray	X-ray ^a		X-ray
Mo-CNT ^b	2.0150(2)	2.019(5)	2.013(1)	2.0100(2)	1.9992(4)	2.0036(4)	2.0096(3)
Mo-P(1)	2.3832(6)	2.385(5)	2.377(4)	2.4656(7)	2.4720(14)	2.4744(15)	2.4801(8)
Mo-P(2)	2.3801(6)	2.377(5)	2.375(4)	2.4720(7)	2.4738(14)	2.4726(15)	2.4685(9)
Mo-H(1)	1.58(3)	1.712(8)		1.67(3)	1.65(4)	1.60(4)	1.83(3)
Mo-H(2)	1.57(3)	1.719(9)		1.58(3)	1.52(4)	1.56(4)	
Mo-H(3)	1.58(3)	1.719(9)		1.61(3)	1.54(4)	1.60(4)	
Mo-H(4)				1.66(3)			
H(2)···H(3)	1.63(4)	1.69(2)			1.33(6)	1.38(6)	
CNT-Mo-P(1)	130.62(2)	130.7(2)	133.8(1)	120.339(18)	127.80(4)	126.13(4)	122.02(2)
CNT-Mo-P(2)	132.14(2)	132.1(2)	131.5(1)	120.808(18)	127.16(4)	127.74(4)	121.57(2)
CNT-Mo-H(1)	106(1)	105.8(3)		108.5(9)	105(2)	104(2)	125.2(9)
CNT-Mo-H(2)	107(1)	106.0(3)		104.9(9)	107(2)	110(2)	
CNT-Mo-H(3)	114(1)	115.1(3)		104.7(9)	106(2)	109(2)	
CNT-Mo-H(4)				173.1(9)			
P(1)-Mo-P(2)	93.71(2)	93.6(2)	94.02(14)	112.09(2)	100.25(6)	100.42(6)	109.55(3)
H(2)-Mo-H(3)	62(2)	58.9(5)			51(2)	52(2)	

^aThe parameters of each crystallographically independent molecule are shown in separate columns. ^bCNT is the centroid of the Cp ring.

Table 2. Crystal data and structure refinement for all structurally characterized complexes

Identification code	2a (X-ray)	2a (neutron)	2b	3a	2a⁺	5a
Empirical formula	C ₂₃ H ₅₀ MoP ₂	C ₂₃ H ₅₀ MoP ₂	C ₂₃ H ₅₀ MoP ₂	C ₂₃ H ₅₁ BF ₄ MoP ₂	C ₂₃ H ₅₀ F ₆ MoP ₃	C ₂₃ H ₄₈ F ₆ MoP ₃
Formula weight	484.51	484.51	481.49	572.33	629.48	627.46
Temperature, K	180(2)	20(1)	180(2)	180(2)	180(2)	180(2)
Wavelength, Å	0.71073	0.37–8.8	0.71073	0.71073	0.71073	0.71073
Crystal system	Monoclinic	Monoclinic	Monoclinic	Monoclinic	Monoclinic	Monoclinic
Space group	P 2 ₁ /n	P 2 ₁ /n	P 2 ₁ /c	P 2 ₁ /c	P 2 ₁ /c	P 2 ₁ /c
a, Å	16.2915(15)	16.238(5)	15.599(4)	9.3986(5)	14.0847(10)	9.6185(5)
b, Å	17.4655(16)	17.392(5)	10.2114(18)	16.9428(8)	26.216(2)	16.8699(10)
c, Å	9.2144(8)	9.160(4)	16.939(4)	18.2340(9)	20.1855(15)	18.7489(12)
α, °	90.0	90.0	90.0	90.0	90.0	90.0
β, °	92.651(10)	92.83(1)	103.51(2)	92.719(4)	99.221(8)	90.441(5)
γ, °	90.0	90.0	90.0	90.0	90.0	90.0
V, Å ³	2619.1(4)	2584(2)	2623.5(10)	2900.3(3)	7357.2(10)	3042.2(3)
Z	4	4	4	4	8	4
D _{calc} , Mg/m ³	1.229	1.246	1.227	1.311	1.269	1.370
μ, mm ⁻¹	0.629	0.0655+0.0002λ	0.628	0.597	0.535	0.636
Crystal size, mm ³	0.27x0.23x0.2	2.2 x 1.6 x 1.4	0.13x0.1x0.1	0.25x0.21x0.13	0.2x0.1x0.1	0.58x0.42x0.24
θ°, range	2.49 to 26.18	8.52 to 81.95	3.17 to 23.20	2.76 to 28.22	2.14 to 25.00°	3.25 to 26.37
Reflections collected	20750	8686	14396	24326	50093	27114
Indpnt refl [R _{int}]	5171 [0.0337]	3203 [0.141]	3766 [0.1239]	7190 [0.0392]	12934 [0.0853]	18993 [0.0513]
Absorption correction	Multi-scan	Gaussian	Multi-scan	Multi-scan	Multi-scan	Multi-scan
Max. and min. transm.	0.8299, 0.7768	1.5609, 1.626	1.0214, 0.8735	0.9996, 0.8209	0.8843, 0.8674	0.8363, 0.7206

Refinement method	F ²	F ²	F ²	F ²	F ²	F ²
Data / restraints / parameters	5171 / 0 / 262	3203 / 0 / 686	3766 / 204 / 249	7190 / 0 / 308	12934 / 216 / 763	18993 / 0 / 317
GOF on F ²	1.034	1.023	1.129	1.013	0.835	1.070
R1, wR2 [I>2σ(I)]	0.0270, 0.0657	0.0603, 0.1542	0.1029, 0.2176	0.0333, 0.0788	0.0488, 0.1052	0.0507, 0.1428
R1, wR2 (all data)	0.0357, 0.0708	0.0608, 0.1546	0.1592, 0.2396	0.0508, 0.0901	0.0963, 0.1174	0.0599, 0.1554

Synopsis

Sterically protecting cyclopentadienyl ligands in combination with PMe_3 yield relatively stable paramagnetic half-sandwich trihydride complexes of molybdenum, showing evidence of an incipient H-H interaction. Subsequent H_2 elimination yields a stable spin quartet 15-electron hydride complex, providing the first well defined example of an oxidatively induced reductive elimination of dihydrogen.

Table of Contents Graphics

